Microporous and Mesoporous Materials 198 (2014) 82–91

Contents lists available at ScienceDirect

Microporous and Mesoporous Materials

journal homepage: www.elsevier.com/locate/micromeso

Oxidative dehydrogenation of propane with nitrous oxide over Fe–O–Al species occluded in ZSM-5: Reaction and deactivation mechanisms

Guangjun Wu [a], Yao Hao [a], Nan Zhang [a], Naijia Guan [a], Landong Li [a,*], Wolfgang Grünert [b,*]

[a] Key Laboratory of Advanced Energy Materials Chemistry (Ministry of Education), College of Chemistry, Nankai University, Tianjin 300071, PR China
[b] Lehrstuhl für Technische Chemie, Ruhr-Universität Bochum, D-44780 Bochum, Germany

ARTICLE INFO

Article history:
Received 10 May 2014
Received in revised form 9 July 2014
Accepted 16 July 2014
Available online 24 July 2014

Keywords:
Fe-ZSM-5
ODHP
Nitrous oxide
Reaction mechanism
Deactivation

ABSTRACT

Fe-ZSM-5 was prepared via solid-state exchange method using ferrocene as iron precursor and applied as a model catalyst to investigate the reaction and deactivation mechanisms of the oxidative dehydrogenation of propane (ODHP) with nitrous oxide. Characterization results reveal that after severe calcination highly isolated Fe–O–Al species are the only exposed iron sites detectable, which account for *ca.* 60% of the total iron species in Fe-ZSM-5. Results from temperature-programmed experiments and in situ DRIFT spectroscopy suggest that the chemisorption of nitrous oxide on Fe–O–Al species leads to the formation of stable mono-oxygen species, which can react with gaseous propane to produce propylene with high selectivity. The accumulation of organic species in the catalyst is observed during the reaction, and the major organic species are determined to be alkylbenzenes. The accumulation rate and the specific constitution of alkylbenzenes are found to depend on the relative partial pressures of propane and nitrous oxide: lower N_2O/C_3H_8 ratios result in formation of aromatics with smaller kinetic diameter, which are accumulated at a lower rate. This leads to lower deactivation rates and longer catalyst lifetimes. Remarkably, a superior stable propane conversion rate of *ca.* 13 mmol g_{cat}^{-1} h^{-1} and a propylene production rate of *ca.* 6 mmol g_{cat}^{-1} h^{-1} can be kept for >40 h with a N_2O/C_3H_8 ratio of 1:2.

1. Introduction

Light olefins are very important components for the petrochemical industry with increasing market demands in recent years. The oxidative dehydrogenation of light alkanes provides a promising route to produce light olefins, and has therefore been widely studied. During the oxidative dehydrogenation of light alkanes with dioxygen, carbon oxides (CO and CO_2) are extensively formed by over-oxidation even at moderate alkane conversions, resulting in low olefin selectivity and olefin yield [1]. Recently, it has been proposed to use nitrous oxide instead of dioxygen as oxidant, and the oxidative dehydrogenation of alkanes with N_2O has attracted considerable attention [2–13]. Iron-zeolites have been developed as unique catalysts for the oxidative dehydrogenation of light alkanes with N_2O, especially the oxidative dehydrogenation of propane to propylene (ODHP).

Despite considerable research effort with respect to ODHP with N_2O over iron-zeolites, some problems are still to be solved before the further development of this reaction. First of all, the reaction mechanism of the ODHP with N_2O is not quite clear yet. In the past decades, activation and conversion of nitrous oxide on iron-zeolites have been extensively investigated [14–19]. In the case of the ODHP with N_2O, the presence of the propane reductant in the reaction system makes the conversion of nitrous oxide on iron-zeolites much more complicated. For the design of effective catalysts, it is important to know the different pathways for the formation of the dehydrogenation product propylene and of by-products. Another essential problem is the deactivation mechanism of catalysts in the ODHP with N_2O. Catalyst deactivation is a key issue in the reaction of oxidative dehydrogenation, no matter whether dioxygen or nitrous oxide is used as oxidant. In a general sense, formation and deposition of coke on the catalyst surface are responsible for catalyst deactivation. However, the specification of coke and its origin are not fully understood. Accordingly, there is no effective means to prevent the deposition of coke and to increase the catalyst lifetime in the ODHP with N_2O.

In our previous work, Fe-ZSM-5 prepared via a solid-state exchange method using ferrocene as iron precursor has been found to exhibit superior performance for the ODHP with N_2O after a severe calcination. A maximal initial propylene yield of 30% at a high turnover frequency of 0.037 s^{-1} could be obtained [20]. Fe–O–Al species were identified as the active sites. Their simple

* Corresponding authors. Tel./fax: +86 22 2350 0341.
E-mail addresses: lild@nankai.edu.cn (L. Li), w.gruenert@techem.rub.de (W. Grünert).

http://dx.doi.org/10.1016/j.micromeso.2014.07.032
1387-1811/

constitution and the almost complete absence of Brønsted acid sites make this Fe-ZSM-5 material an ideal model catalyst for studying the ODHP with N_2O. The present work aims to present a detailed study on this reaction over Fe-ZSM-5, with emphasis on the reaction and deactivation mechanism.

2. Experimental

2.1. Sample preparation

ZSM-5 zeolite in its H-form (Sinopec, Si/Al = 24, Fe impurity: ~60 ppm) was employed as host for iron species. Fe-ZSM-5 was prepared by solid-state exchange using ferrocene as iron source [21]. In a typical experiment, *ca.* 3 g of the zeolite was placed in a quartz reaction chamber connected to a vacuum line and treated at $5 * 10^{-2}$ Pa and 573 K for 4 h. After cooling to 323 K, the reaction chamber was transferred into a glove box and 0.5 g ferrocene was dumped onto the dried zeolite. Subsequently, the chamber was heated to 423 K and kept at this temperature under vacuum for 24 h to insure the complete surface reaction between ferrocene and the zeolite Brønsted acid sites. The resulting solid was calcined in flowing air (H_2O level of ~200 ppm) at 1073 K for 6 h. It will be denoted as Fe-ZSM-5-G. For reference, Fe-ZSM-5 was also prepared by conventional solid-state ion exchange using $FeCl_3$ as iron precursor. In a typical experiment, 1 g zeolite sample was mechanically mixed with 0.5 g $FeCl_3$ in the glove box and the mixture was placed in a sealed reactor. The reactor was heated to 573 K at 10 K/min and kept at this temperature for 2 h. The resulting solid was thoroughly washed with deionized water, dried at 353 K overnight and calcined in flowing air at 1073 K for 6 h. The product will be denoted as Fe-ZSM-5-E.

2.2. Sample characterization

FTIR spectra in diffuse reflection mode, *i.e.* DRIFTS, with the probe molecule NO were collected on a Bruker Tensor 27 spectrometer (64 scans, resolution – 2 cm^{-1}). A self-supporting pellet made of the catalyst sample was placed in the reaction chamber (Harrick, Praying Mantis CHC-CHA-3) and pretreated in flowing He at 773 K for 1 h. After cooling to room temperature in flowing He, the He stream was switched to 1%NO/He and a series of time-dependent DRIFT spectra were recorded, which will be reported in terms of the Kubelka–Munk (K–M) function below.

Si, Al and Fe contents in the samples were analyzed by a Perkin Elmer Optima 2000 inductively coupled plasma optical emission spectrometer (ICP-OES). The samples were dissolved in hot aqua regia with the addition of several drops of HF. Before ICP analysis, the excess acid in solution was removed by heating at constant temperature of 453 K.

The amounts of organic compounds deposited on Fe-ZSM-5 catalyst after ODHP with N_2O were analyzed by thermogravimetry (TG) on a Setram Setsys 16/18 thermogravimetric analyzer. In a typical measurement, 0.1 g of Fe-ZSM-5 after 400 min time-on-stream in ODHP was pretreated at 373 K in an Al_2O_3 crucible to remove the physisorbed water/organic and then heated to 1273 K at a constant rate of 10 K min^{-1} and under flowing synthetic air of 30 mL min^{-1}.

The constitution of organic compounds occluded in the channels of Fe-ZSM-5-G catalyst after ODHP with N_2O was analyzed by gas chromatography with mass-spectrometric detection (GC–MS). Typically, 0.3 g catalyst sample after reaction was carefully dissolved in 10 mL 1 M HF solution. The solution was treated with 10 mL CH_2Cl_2 to extract the organic compounds and the residual water was removed by the addition of sufficient sodium sulfate solid. Then, 1.0 μL CH_2Cl_2 organic extract was analyzed by GC–MS (Agilent 7890A/5975 MSD) with a DB-5 MS column (30 m, 0.25 mm i.d., stationary phase thickness 0.25 μm). The following temperature program was employed: isothermal at 313 K for 6 min, heating to 553 K with a rate of 10 K min^{-1}, and isothermal at 553 K for 10 min.

2.3. Isothermal transient response experiments

Isothermal transient response experiments were performed in a quartz plug-flow reactor at atmosphere pressure. Pure He was fed to the reactor loaded with a Fe-ZSM-5 sample (pretreated in flowing He at 773 K for 1 h) at 20 mL min^{-1} and transient pulses of pure nitrous oxide (100 μL per pulse) were injected into the feed stream via an electronic six-port valve. The reactor outlet was on-line analyzed by using a quadrupole mass spectrometer (Pfeiffer Omnistar QIC 20).

2.4. Temperature-programmed experiments

Temperature-programmed desorption and surface reaction (abbreviated as TPD and TPSR, respectively) experiments were performed in a quartz plug-flow reactor at atmospheric pressure. Generally, the inlet gas mixture was fed to the reactor through four mass-flow controllers (Seven Star D-07) and the reactor outlet was analyzed by using a quadrupole mass spectrometer (MS) in the multiple-ion detection mode. The following main mass fragments (*m*/*e*) were recorded: 4 (He), 18 (H_2O), 28 (N_2, N_2O, CO), 30 (N_2O), 32 (O_2), 40 (Ar), 43 (C_3H_6), 44 (N_2O, CO_2), 45 (C_3H_8), 56 (acrolein), 58 (allyl alcohol), 91 (toluene, MB), 105 (xylene, DMB) and 106 (ethylbenzene, EB). The presence of NO and NO_2 under our reaction conditions could be excluded according to the results from a chemiluminescence NO_x analyzer (Ecotech EC 9841). Calibration was carried out with mixtures of known gas composition. If more than one component contributed to a mass fragment, a second mass was used to distinguish the different components.

For TPSR, the catalyst sample was pretreated in He at 773 K for 1 h and cooled to 473 K in flowing He. The catalyst was then contacted with the reactant gas mixture (N_2O/He or N_2O/C_3H_8/He) for 30 min, subsequently TPSR was performed from 473 to 873 K at a heating rate of 10 K min^{-1} and the reaction outlet was monitored by an on-line MS. For TPD, the catalyst sample was also pretreated in He at 773 K for 1 h and cooled to 473 K in flowing He. After the saturated adsorption of N_2O/He or O_2/He at 473 K, the sample was cooled to 373 K and purged with He for 30 min. Finally, TPD was performed in flowing He from 473 to 873 K at a heating rate of 10 K min^{-1} and the outlet was monitored by on-line MS.

2.5. In situ DRIFTS study

In situ DRIFT spectra were recorded on the Bruker Tensor 27 spectrometer, equipped with a liquid N_2 cooled MCT detector. The catalyst samples of *ca.* 25 mg were finely ground and placed in the reaction chamber (Harrick, Praying Mantis CHC-CHA-3). Prior to each experiment, the sample was pretreated in He at 773 K for 1 h and cooled to the desired temperature for taking a reference spectrum. Then, the designed reaction gas mixture was fed to the sample and DRIFT spectra were recorded (128 scans at a resolution of 4 cm^{-1}).

2.6. Steady-state catalytic reaction

The catalytic evaluation was performed in a fixed-bed flow micro-reactor at atmospheric pressure. Typically, 0.2 g catalyst sample (sieve fraction of 0.17–0.25 mm, *ca.* 0.2 mL) was placed in a quartz reactor (4 mm i.d.) and pretreated in He at 773 K for 1 h. After cooling to designed temperature, the reactant gas mixture ($C_3H_8 + N_2O$ = 22.5%, He balance, realized by three independent

mass-flow controllers for C_3H_8, N_2O and He) was fed to a total flow rate of 50 mL min^{-1}, corresponding to a gas hourly space velocity (GHSV) of 15,000 h^{-1}. The reaction was conducted isothermally and the gas products were analyzed by using two on-line gas chromatographs. One of them was equipped with a Plot Q capillary column and a FID detector for the analysis of organic products, the other with two packed columns (Porapak Q and Carbon Molecular Sieve TDX) and a TCD detector for the analysis of N_2O, N_2, O_2 and CO_x. The water was removed from the gas products before the chromatograph inlet and a possible small change of the reaction volume was neglected in the formulas used for conversion, selectivity and yield calculations.

3. Results

3.1. Characterization of active iron sites

The physicochemical properties of Fe-ZSM-5 employed in this study have been characterized by a series of techniques, *e.g.* XRD, ^{27}Al-MAS-NMR and NH_3-TPD, and the Fe sites have been studied by means of UV–Vis, TEM, and H_2-TPR. For conciseness, some characterization results are shown in the Supporting information (Figs. S1–S6), and detailed analysis of results can be found in our previous work [20]. Briefly, framework Al species dominate in Fe-ZSM-5-G (^{27}Al-MAS-NMR, Fig. S2) and the almost complete absence of Brønsted acid sites (NH_3-TPD, Fig. S3) indicates the attachment of iron species to aluminum via oxygen. The iron species in Fe-ZSM-5-G exist in the form of isolated ferric ions or oligonuclear Fe_xO_y clusters (UV–Vis, Fig. S4), which are almost invisible in the TEM (Fig. S5). This is also confirmed by the reduction of ferric ions to ferrous ions by hydrogen (H/Fe = 1.2) in the temperature range of 400–900 K (H_2-TPR, Fig. S6). A summary of relevant physicochemical properties of Fe-ZSM-5 under study is displayed in Table 1.

FTIR spectroscopy with NO probe is an efficient technique for the characterization of exposed iron sites in zeolites. It is sensitive to ferrous ions due to the preferential interaction of NO with Fe^{2+} [22–24]. Therefore, our Fe-MFI samples previously calcined in air were further treated at elevated temperature (773 K) under inert atmosphere to induce the auto-reduction of ferric ions to ferrous ions (No obvious adsorption of NO on iron sites was observed without auto-reduction pre-treatment) [25,26]. Fig. 1 shows the DRIFT spectra of NO adsorption on Fe-ZSM-5 samples at room temperature. NO adsorption on Fe-ZSM-5-G results in an obvious IR band at 1875 cm^{-1}, which has been ascribed to mono-nitrosyls on Fe^{2+}–O–Al nanoparticles in literature [27]. However, considering that nanoparticles are scarce in our Fe-ZSM-5-G sample (UV–Vis, Fig. S4; TEM, Fig. S5), we prefer to ascribe the band at 1875 cm^{-1} to mono-nitrosyls on rather isolated Fe^{2+}–O–Al species. The intensity of this band increases dramatically at the initial stage up to 3 min, and then decreases gradually with the further extension of adsorption time. Meanwhile, several IR bands at 1645, 1615 and 1580 cm^{-1} corresponding to nitro and nitrate species [22,28] appear due to the oxidation of mono-nitrosyls by residual oxygen, either from NO gas or from the Fe-ZSM-5 sample, and their intensities gradually increase with the extension of adsorption time. Obviously, Fe^{2+}–O–Al species are present as exclusive detectable iron species in Fe-ZSM-5-G after treatment in He at 773 K. NO molecules are initially adsorbed on Fe^{2+}–O–Al species in the form of nitrosyls and then gradually transformed into nitro and nitrate species (see Table 2).

Table 1
Physicochemical properties of Fe-ZSM-5 under study.

Fe-zeolite	Si/Al[a]	Fe (%)	Fe/Al[a]	S_{BET} (m^2/g)
Fe-ZSM-5-G[b]	23.7	1.82	0.48	423
Fe-ZSM-5-G	24.5	0.62	0.17	436
Fe-ZSM-5-E[b]	23.2	2.65	0.69	402
Fe-ZSM-5-E	23.6	2.53	0.66	372

[a] Molar ratio.
[b] Uncalcined sample after surface reaction between ferrocene and the zeolite Brønsted acid sites at 423 K.

In the case of Fe-ZSM-5-E, NO adsorption results in two IR bands at 1875 and 1845 cm^{-1} in the nitrosyl region. While the band at 1875 cm^{-1} arises from the Fe^{2+}–O–Al species just mentioned [24,27], the band at 1845 cm^{-1} has been assigned to mono-nitrosyls on ferrous ions in the straight channels of ZSM-5 [29,30]. Since the latter band is rather broad in shape, we prefer to attribute it to mono-nitrosyls on ferrous ions in oligonuclear Fe_xO_y clusters in the straight channels of ZSM-5 [27]. With the duration of adsorption, mono-nitrosyls on Fe^{2+}–O–Al species gradually transform into nitro and nitrate species (IR bands at 1675, 1640, 1605 and 1580 cm^{-1}) and mono-nitrosyls on oligonuclear clusters accumulate to some extent. Based on the DRIFT spectra of NO adsorption on Fe-ZSM-5-G and Fe-ZSM-5-E, it is quite evident that different iron sites are formed in Fe-ZSM-5 prepared by solid-state ion exchange using different iron precursors, *i.e.* ferrocene and $FeCl_3$.

The amount of ferrous sites in Fe-ZSM-5 accessible to the gas phase was quantitatively analyzed by pulse adsorption of N_2O on activated samples, based on the method employed in literature [31–33]. Fig. 2 shows that N_2O and N_2 signals can be observed in the outlet when nitrous oxide pulses were administered to the Fe-ZSM-5 sample at 473 K, while no molecular dioxygen was detected at the outlet during the whole process. The concentration of accessible iron sites can be measured from both the amount of N_2 released and the amount of N_2O consumed. The density of accessible iron sites was estimated to be $4.3 * 10^{19}$ and $5.2 * 10^{19}$ $g^{-1}$for Fe-ZSM-5-G and Fe-ZSM-5-E, respectively. Related to the total iron contents, *ca.* 60% of total iron species are accessible ferrous sites in Fe-ZSM-5-G, while only *ca.* 20% total iron species are accessible ferrous sites in Fe-ZSM-5-E. This confirms that the iron species in Fe-ZSM-5-G are extremely disperse, *i.e.* isolated Fe–O–Al species.

3.2. TPSR and TPD results

Fig. S7 shows the TPSR results of N_2O decomposition over Fe-ZSM-5. It is seen that both Fe-ZSM-5-E and Fe-ZSM-5-G are active catalysts for this reaction. Typically, N_2O conversion starts at 650 and 700 K for Fe-ZSM-5-E and Fe-ZSM-5-G, respectively, and the overall decomposition of nitrous oxide can be obtained at *ca.* 800 K for both catalysts.

The TPSR results of ODHP with N_2O over Fe-ZSM-5 catalysts are shown in Fig. 3. The presence of propane in the reaction system greatly promotes N_2O conversion at relative low temperatures of <650 K. Propane conversion over Fe-ZSM-5 first increases with the reaction temperature, reaches a maximum at *ca.* 725 K, and then begins to decrease. Propylene and CO_x (CO and CO_2) are observed as the main products from the oxidation of propane catalyzed by both Fe-ZSM-5-E and Fe-ZSM-5-G. A much higher percentage of propylene is observed over Fe-ZSM-5-G than that over Fe-ZSM-5-E, indicating the higher propylene selectivity in the ODHP with N_2O over Fe-ZSM-5-G. This should be due to the absence of Brønsted acid sites and Fe_xO_y nanoparticles, which contribute to the deep oxidation of propane to CO_x.

Besides the desired product propylene and main by-products CO_x, traces of other by-products can be detected from the ODHP with N_2O, as shown in Fig. 4. Aromatics (MB, DMB and EB), allyl alcohol and acrolein are detected over Fe-ZSM-5-G, while aromatics (MB, DMB and EB) and acrolein are found over Fe-ZSM-5-E. The aromatics should originate from an aromatization reaction, and

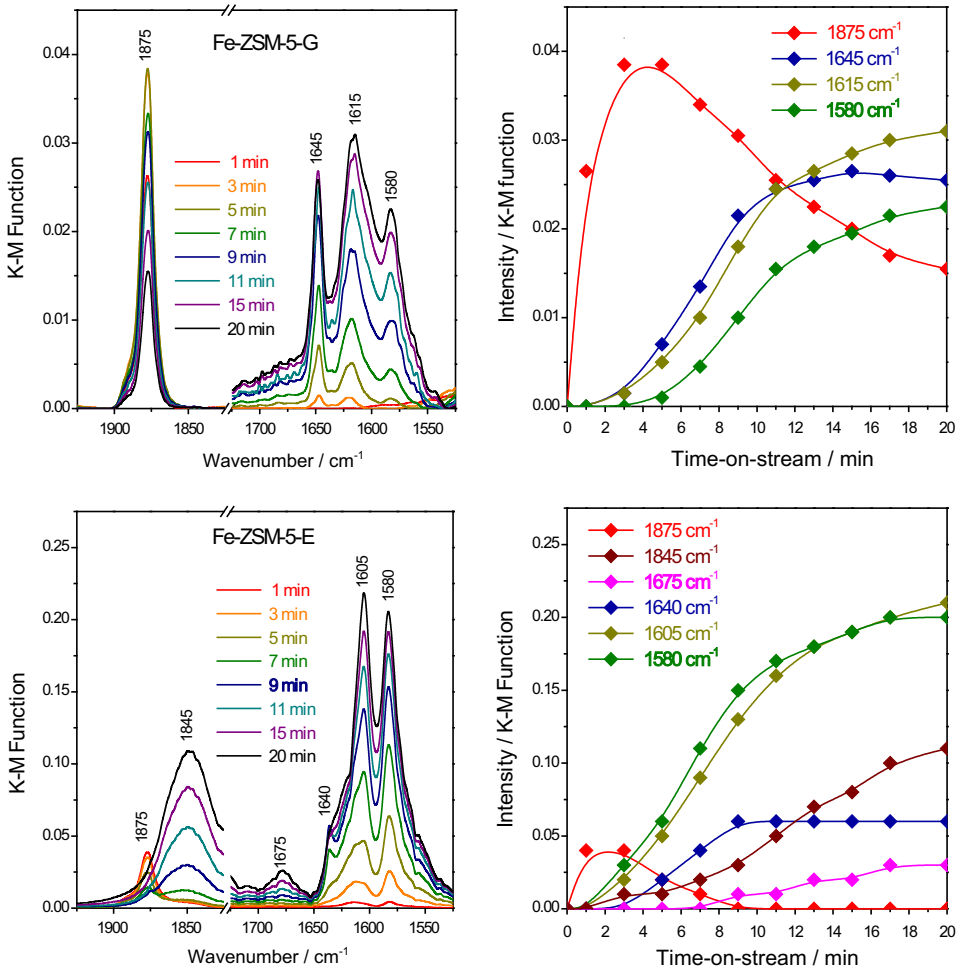

Fig. 1. DRIFT spectra of NO adsorption on Fe-ZSM-5-G and Fe-ZSM-5-E, and the development of IR bands during NO adsorption.

Table 2
Summary of IR bands observed during nitrous oxide and propane adsorption on Fe-ZSM-5.

Origination	Wavenumber (cm^{-1})	Assignment
N_2O adsorption	3495 and 3465 2580 and 2550 2235 and 2205 1305 and 1270	Gas-phase N_2O
	3740 ~3450	ν_{O-H} of Si–OH ν_{O-H} of OH interacting with adsorbates
C_3H_8 adsorption	~2970 1605 1470	ν_{C-H} of R–CH_3 and R–CH_2 ν_{C-O} of bicarbonates δ_{C-H} of R–CH_3

they will probably contribute to coke formation on the catalyst. Allyl alcohol and acrolein should originate from the further oxidation of the reaction product propylene [34,35].

The profiles of O_2-TPD from Fe-ZSM-5-G and Fe-ZSM-5-E previously oxidized with O_2 or with N_2O are shown in Fig. 5. Although the profiles provide us with a very complicated and even distorted picture due to the secondary transformation of adsorbed oxygen species, some very important issues can be explored. For Fe-ZSM-5-E, multiple desorption peaks are observed in the 700–1050 K temperature range from the sample oxidized in O_2 (O/Fe = 0.09), while the sample reoxidized in N_2O produces desorption peaks in a wider temperature range (550–1150 K, O/Fe = 0.11). These results are consistent with those reported by Kunimori et al. [36], and the O_2 desorption peak below 700 K obtained after contact with N_2O might be related to the highly reactive so-called α-oxygen species [37]. For Fe-ZSM-5-G oxidized in O_2, desorption peaks are observed in the 750–1050 K temperature range as well (O/Fe = 0.10), similar to those on Fe-ZSM-5-E. Surprisingly, the O_2 signals obtained after reoxidation of this sample in N_2O are very weak: O/Fe was just 0.035. The oxygen species adsorbed by the ferrous sites in Fe-ZSM-5-G upon interaction with N_2O should be consumed in the reoxidation of iron sites, but apparently it transforms to an oxygen species with surprising stability.

To further examine this phenomenon, DRIFT spectra of NO adsorbed on Fe-ZSM-5-G after reoxidation by N_2O and another auto-reduction treatment (N_2O treatment at 773 K for 1 h followed by He treatment at 773 K for 1 h) were measured, and the results are given in Fig. S8. Again the signal at 1875 cm^{-1} corresponding to mono-nitrosyls on Fe^{2+}–O–Al species is dominant, similar to those observed for Fe-ZSM-5-G with simple auto-reduction treatment (Fig. 1). However, the relative intensity of signal, reflected by the signal/noise ratio, is much lower, indicating that a large proportion of the iron species oxidized by nitrous oxide could not be reduced through treatment in He at 773 K, consistent with the TPD result. Obviously, the newly formed oxygen species could survive the high temperature auto-reduction process to a large extent.

Based on literature reports, two types of oxygen species have been identified for nitrous oxide activation over iron-zeolite: highly active α-O and thermally stable mono-oxygen [5,38]. In

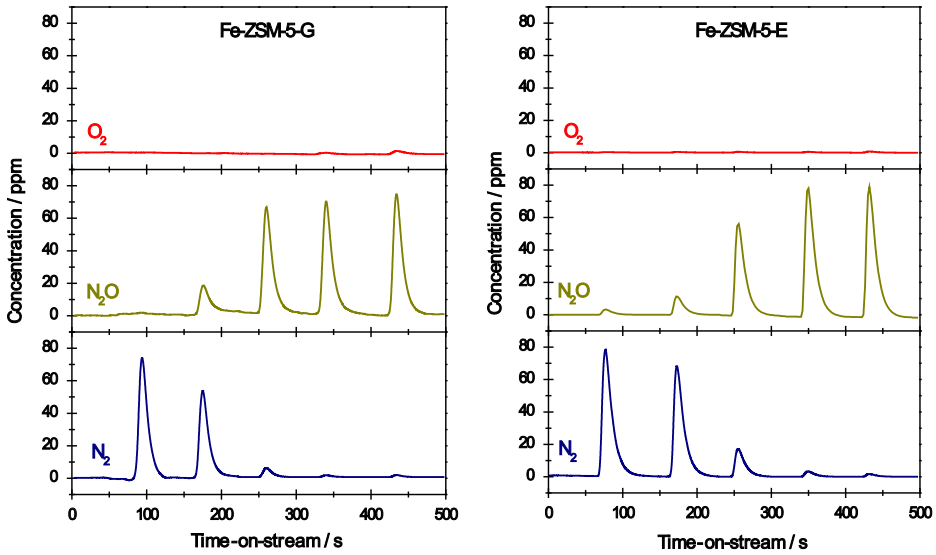

Fig. 2. Responses to nitrous oxide pulses onto Fe-ZSM-5-G and Fe-ZSM-5-E at 473 K.

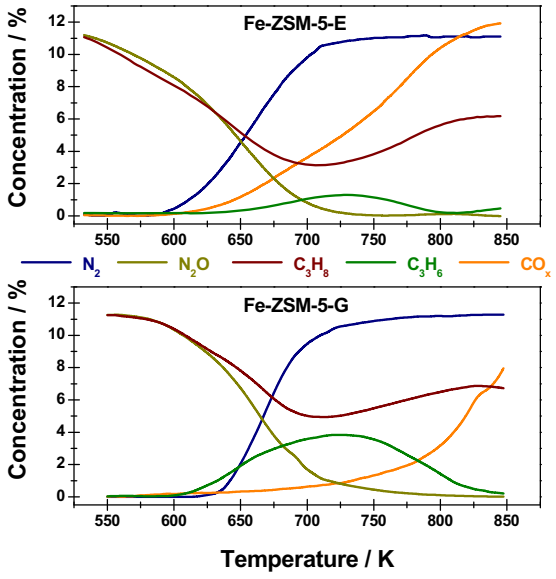

Fig. 3. TPSR of the ODHP with nitrous oxide over Fe-ZSM-5-G and Fe-ZSM-5-E. Reaction conditions: $N_2O + C_3H_8 \approx 22.5\%$, He balance, GHSV = 15,000 h^{-1}.

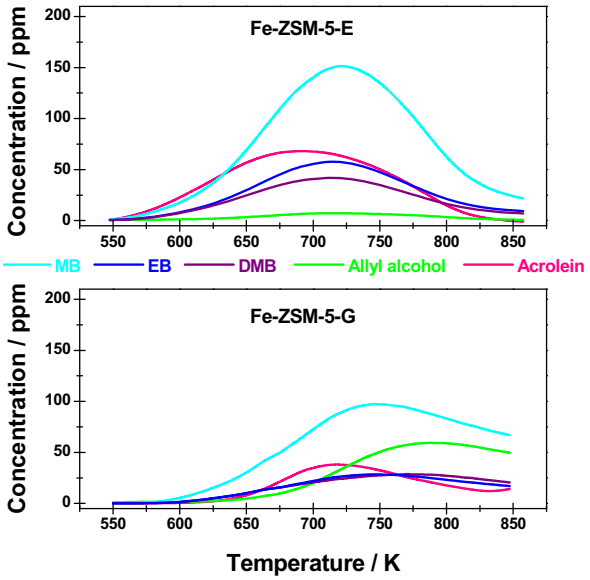

Fig. 4. Traces of by-products in the TPSR of the ODHP with nitrous oxide over Fe-ZSM-5-G and Fe-ZSM-5-E.

the present study, the oxygen species deposited on the iron sites in Fe-ZSM-5-G should be thermally stable mono-oxygen based on their origin and properties [37,39]. However, the oxygen species are somewhat different to those reported in literature [5,38]. On the one side, they are stable and can survive the high temperature treatment to a large extent, probably due to the reduced mobility of oxygen species on highly isolated iron sites. On the other side, they are reactive towards propane and can lead to oxidative dehydrogenation according to our catalytic results (Fig. 3).

3.3. In situ DRIFT spectroscopy results

The evolution of IR bands observed on Fe-ZSM-5-G under reaction conditions of ODHP with N_2O is shown in Fig. 6. At low temperature of 473 K, where the ODHP reaction does not yet proceed, a series of IR bands in the region of 4000–1000 cm^{-1} can be observed. Typically, the bands at 3495, 3465, 2580, 2550, 2235, 2205, 1305 and 1270 cm^{-1} should be attributed to gas-phase nitrous oxide [40]. The multiple bands at ~2970 cm^{-1} (2970, 2930 and 2875 cm^{-1}) are due to C–H stretching vibrations of –CHx species while the band at 1470 cm^{-1} is due to the bending vibration of –CHx species [40,41]. At high temperature of 748 K, where propylene is produced at a significant rate, all of the above-mentioned IR bands can be observed as well. In addition, a weak negative band at 3740 cm^{-1}, a strong broad band centered at 3450 cm^{-1} and a band at 1605 cm^{-1}appear. The band at 3740 cm^{-1} is due to the O–H stretching vibration of Si–OH [42]. Its negative intensity suggests that Si–OH groups are interacting with adsorbates, which in turn results in the appearance of a broad band of interacting OH groups centered at 3450 cm^{-1}. The band at 1605 cm^{-1} could be due to the C–O stretching vibration of bicarbonate anions [43].

To obtain further information on the reaction process of ODHP with N_2O, activation and conversion of nitrous oxide and propane on Fe-ZSM-5-G at 748 K are examined individually by means of in situ DRIFT spectroscopy, as shown in Fig. 7. During N_2O adsorption on Fe-ZSM-5-G at 748 K only the signals of gas-phase N_2O

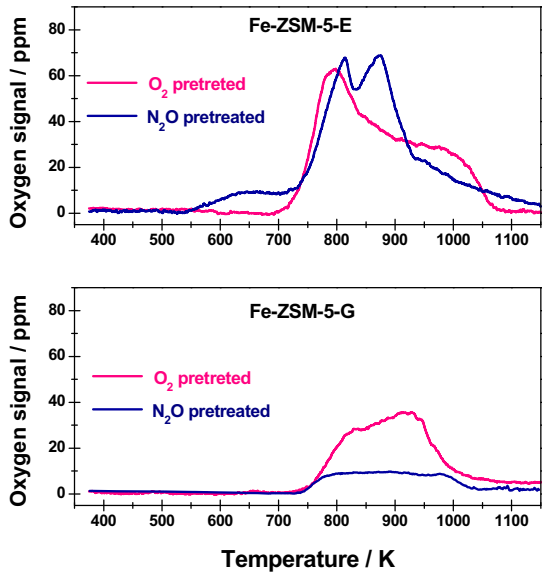

Fig. 5. O_2-TPD profiles of Fe-ZSM-5-G and Fe-ZSM-5-E pretreated in oxygen or nitrous oxide.

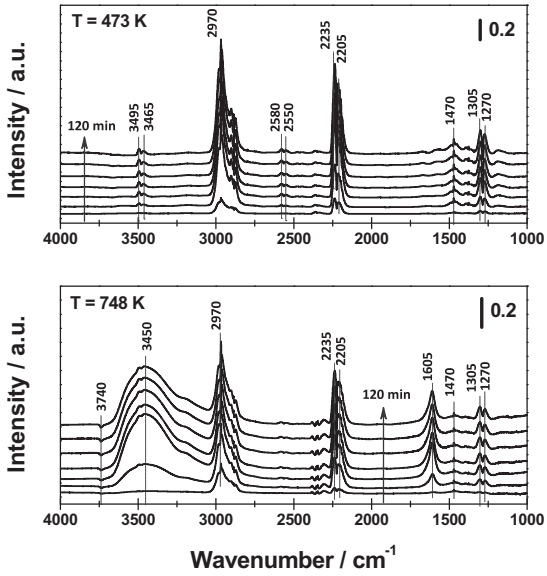

Fig. 6. In situ DRIFT spectra taken during ODHP with nitrous oxide on Fe-ZSM-5-G at 473 and 748 K. Reaction conditions: $N_2O = C_3H_8 \approx 11.2\%$, He balance, GHSV = 15,000 h^{-1}.

(at 3495, 3465, 2580, 2550, 2235, 2205, 1305, and 1270 cm^{-1}) can be detected During subsequent propane purging, the signals of gas-phase N_2O disappear and new bands originated from the activation of propane, *i.e.* R–CHx and bicarbonates, appear. Initial propane adsorption on Fe-ZSM-5-G leads to the formation of R–CHx (IR bands at ~2970 and 1470 cm^{-1}) and bicarbonates (IR band at 1605 cm^{-1}), accompanied by the consumption of Si–OH (IR band at 3740 cm^{-1}). Subsequent purging by N_2O results in the disappearance of all these species and gas-phase N_2O can be observed instead.

Based on these results, it is easily concluded that propane can adsorb on Fe-ZSM-5-G in the form of R–CHx, which can be further oxidized to bicarbonates at 748 K. During this process, the ferric ions could be reduced to ferrous ions. At low temperature of 473 K, propane can also adsorb on Fe-ZSM-5-G in the form of R–CHx while it could not reduce ferric ions to ferrous ions (Fig. S9).

3.4. Steady-state reaction results

Due to its superior performance in TPSR (Fig. 3), the discussion will be focused on Fe-ZSM-5-G in this section. The time-on-stream behavior of Fe-ZSM-5-G in ODHP with N_2O at different temperatures is shown in Fig. 8. It is clearly seen that Fe-ZSM-5-G suffers from severe deactivation during ODHP: propane conversion rate falls gradually from the very beginning of the reaction, consistent with literature reports [4,5,8]. In the 698–773 K temperature range, higher propane conversion is obtained at higher reaction temperature after 100 min time-on-stream. Meanwhile, the propylene selectivity first increases with time-on-stream and then reaches steady states. Higher propylene selectivity is ob served at lower reaction temperature. As a balance of propane conversion and propylene selectivity, the propylene yield first increases to a maximal value and then begins to drop with time-on-stream.

The time-on-stream behavior of Fe-ZSM-5-G in ODHP with N_2O at different N_2O/C_3H_8 ratios is shown for 748 K in Fig. 9. Higher initial propane conversion rate is obtained at higher N_2O/C_3H_8 ratio. At the same time, however, higher N_2O/C_3H_8 ratio results in more severe deactivation. It is interesting to note that the propane conversion rates with N_2O/C_3H_8 ratio of 1:2 (propane conversion: 14.1%) and 2:3 (propane conversion: 16.9%) are very stable and no deactivation can be observed within 400 min time-on-stream. In addition, higher propene selectivity is obtained at lower N_2O/C_3H_8 ratios. Typically, volcanic type curves are observed with N_2O/C_3H_8 ratio of 1:1, 3:2 and 2:1. In contrast, stable propylene selectivity is obtained with N_2O/C_3H_8 ratio of 1:2 and 2:3. As a whole, a maximal propylene production rate of *ca.* 6 mmol g_{cat}^{-1} h^{-1} can be obtained on Fe-ZSM-5-G at 748 K with a N_2O/C_3H_8 ratio of 1:2, and this value can be kept unchanged for as long as 400 min.

We further tested the deactivation and regeneration of Fe-ZSM-5-G under optimized reaction conditions, *i.e.* at a temperature of 748 K and with N_2O/C_3H_8 ratio of 1:2. As shown in Fig. 10, superior stable propane conversion rate of *ca.* 13 mmol g_{cat}^{-1} h^{-1} and propylene production rate of *ca.* 6 mmol g_{cat}^{-1} h^{-1} can be kept for over 40 h. Afterwards, both the propane conversion rate and the propylene production rate begin to drop slightly. A loss of 60% propylene production rate is observed at 64 h time-on-stream. After regeneration in 7.5% N_2O/He at 973 K for 3 h, the catalytic activity of Fe-ZSM-5-G in ODHP with N_2O can recover to the initial level. The regenerated catalyst exhibits similar deactivation behavior as the fresh catalyst, indicating that the Fe-ZSM-5-G catalyst can be continuously regenerated for ODHP with N_2O. To the best of our knowledge, Fe-ZSM-5-G exhibits the highest up-to-date stability in ODHP with N_2O under comparable reaction conditions. Since the deactivation is the most important issue for ODHP, it is reasonable to believe that Fe-ZSM-5-G is good candidate for further research.

3.5. Nature of coke deposited on catalysts

The total amounts of organic species formed on Fe-ZSM-5-G in ODHP with N_2O were analyzed by TG in the temperature range from 323 to 1273 K. More organic species are deposited on the Fe-ZSM-5-G sample at higher N_2O/C_3H_8 ratios (Fig. 11). In the temperature range from 400 to 900 K, the weight losses for Fe-ZSM-5-G are 5.9 wt.% (N_2O/C_3H_8 = 1:2), 7.4 wt.% (N_2O/C_3H_8 = 2:3), 9.6 wt.% (N_2O/C_3H_8 = 1:1), 10.7 wt.% (N_2O/C_3H_8 = 3:2) and 11.8 wt.% (N_2O/C_3H_8 = 2:1), respectively. Considering that more propane is fed to Fe-ZSM-5-G during the 400 min time-on-stream at lower N_2O/C_3H_8 ratio, the rate of "coke" accumulation is distinctly lower with lower N_2O/C_3H_8 ratio. As it is well

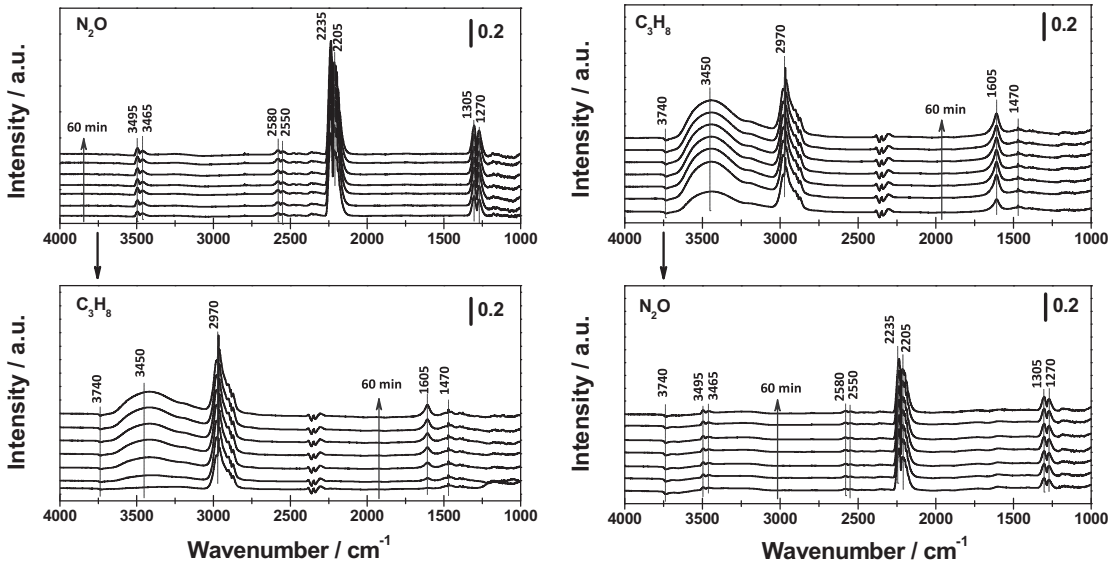

Fig. 7. In situ DRIFT spectra taken during nitrous oxide adsorption followed by purging with propane (left) and propane adsorption followed by purging with nitrous oxide (right) on Fe-ZSM-5-G at 748 K.

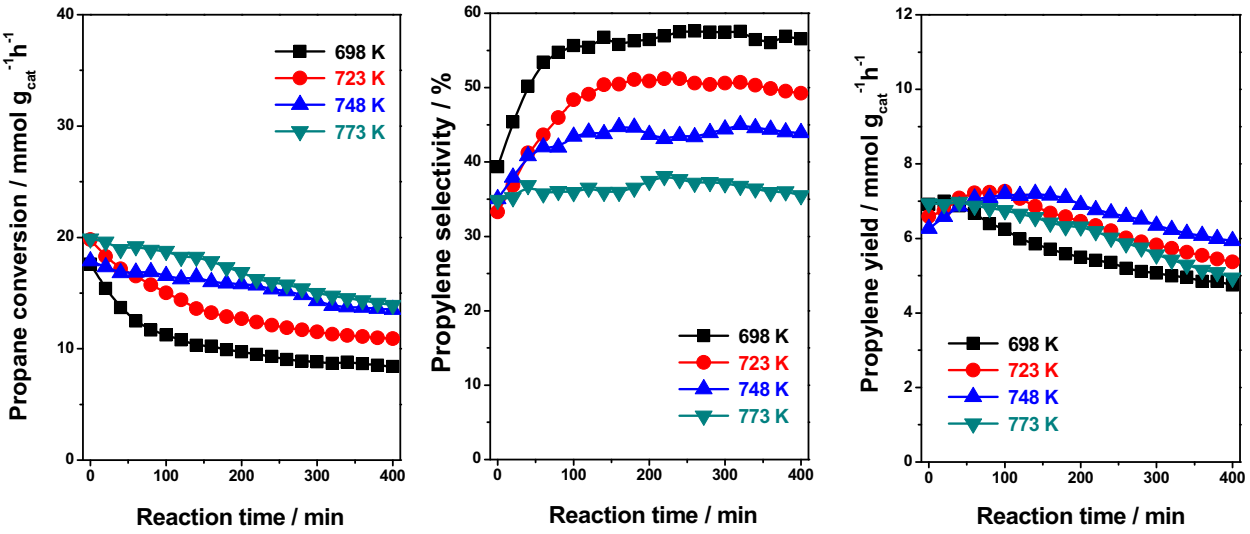

Fig. 8. Propane conversions, propene selectivities and yields during ODHP with nitrous oxide catalyzed by Fe-ZSM-5-G at different temperatures. Reaction conditions: $N_2O = C_3H_8 \approx 11.2\%$, He balance, GHSV = 15,000 h^{-1}.

known that coke formation will cause catalyst deactivation in ODHP, the best catalytic stability and the longest lifetime are expected to be obtained with a N_2O/C_3H_8 ratio of 1:2.

The exact constitution of the bulky organic deposits occluded in the channels of the spent catalyst samples after 400 min time-on-stream has been analyzed by GC–MS after dissolution of catalyst framework and extraction of the organics [44,45]. The peak assignments are made by comparing the related mass spectra with the NIST database [46]. As shown in Fig. 12, mostly alkylbenzene species are formed during ODHP with N_2O over Fe-ZSM-5-G, and these species should come from the aromatization of reactant propane or product propylene [47]. The amount of alkylbenzene species, judged from their relative intensities, increases with increasing N_2O/C_3H_8 ratio, consistent with TG analysis results. Moreover, the specific constitution of alkylbenzene species varies with the N_2O/C_3H_8 ratio. Toluene is formed at the N_2O/C_3H_8 ratio of 1:2, while xylene and ethylbenzene are formed at the N_2O/C_3H_8 ratio of 2:1. Obviously, the kinetic diameter of aromatics occluded in the channels of Fe-ZSM-5-G increases with increasing N_2O/C_3H_8 ratio, *i.e.* from *ca.* 0.59 nm (toluene and p-xylene) to *ca.* 0.62 nm (ethylbenzene) and *ca.* 0.68 nm (o-xylene and m-xylene). It is well known that toluene and p-xylene could diffuse through the channels of MFI structure (0.51×0.57 nm), while o-xylene and m-xylene could not [48,49]. Therefore, o-xylene and m-xylene with large kinetic diameter have to be confined within the intersection of the straight and sinusoidal channels, which results in the blocking of channels and accelerates the accumulation of organic species.

4. Discussion

4.1. Reaction mechanism for ODHP with nitrous oxide

During the past decades, the mechanism of nitrous oxide decomposition over Fe-zeolites has been extensively studied and

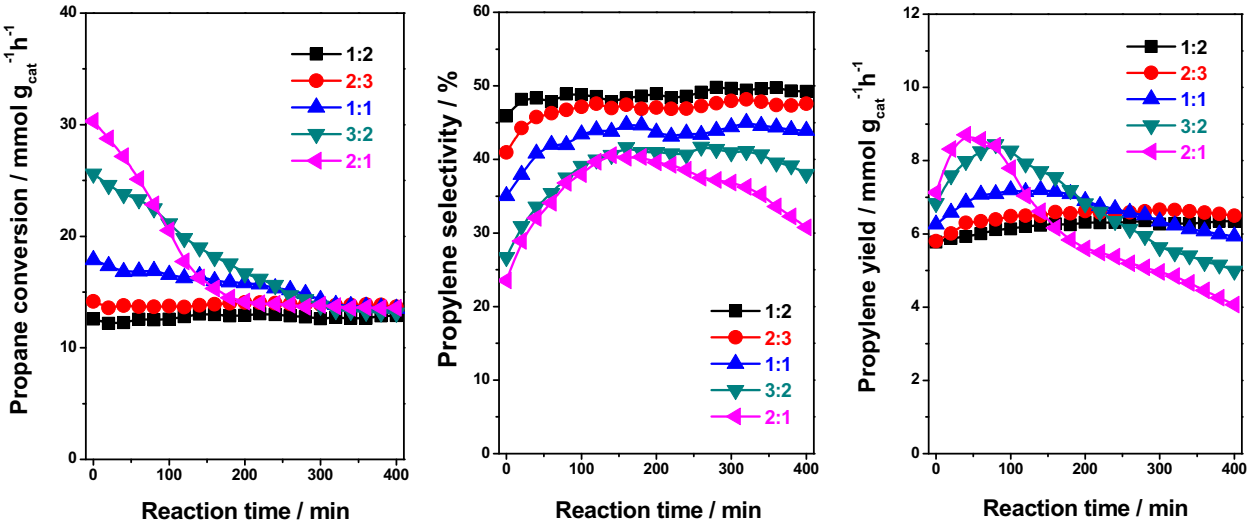

Fig. 9. Propane conversions, propene selectivities and yields during ODHP with nitrous oxide catalyzed by Fe-ZSM-5-G at 748 K with different N_2O/C_3H_8 ratios. Reaction conditions: $N_2O + C_3H_8 \approx 22.5\%$, He balance, GHSV = 15,000 h^{-1}.

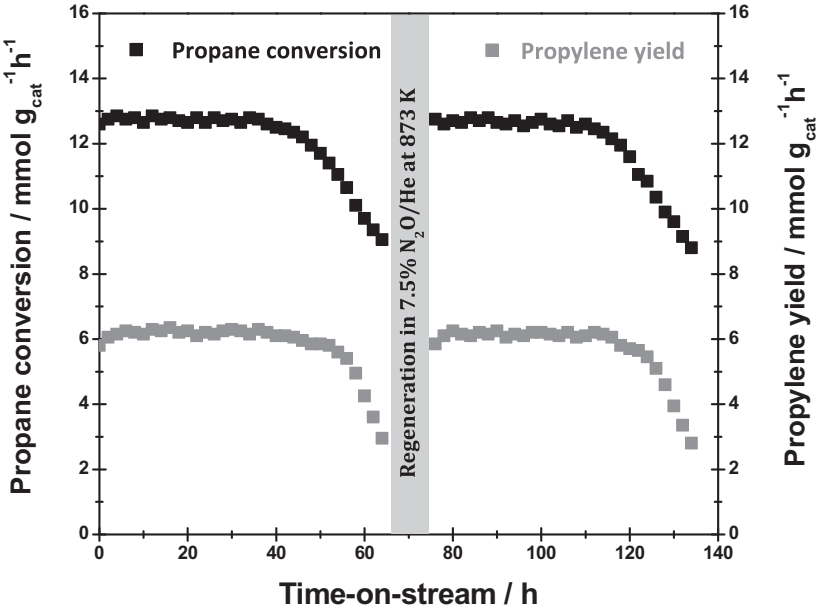

Fig. 10. Deactivation and regeneration of Fe-ZSM-5-G catalyst in the ODHP with nitrous oxide at 748 K. Reaction conditions: 7.5% N_2O, 15% C_3H_8, He balance, GHSV = 15,000 h^{-1}.

the following simplified mechanism is widely accepted (* indicates the active site) [50,33]:

$$N_2O + * \rightarrow N_2 + * - O \quad (R1)$$

$$2* - O \rightarrow O_2 + 2* \quad (R2)$$

$$N_2O + * - O \rightarrow N_2 + * - O_2 \rightarrow N_2 + O_2 + * \quad (R3)$$

In the present study, highly isolated Fe–O-Al species are detected as in Fe-ZSM-5-G, and, therefore, the Eley–Rideal mechanism (R3) should be the dominating process for nitrous oxide decomposition over Fe-ZSM-5-G. More specifically, the Fe^{3+}–Fe^{2+} cycle operates and N_2O decomposes to N_2 and O_2 continuously (R4, R5, R6, R7).

$$Fe^{2+} + N_2O \rightarrow N_2 + Fe^{2+} - O \quad (R4)$$

$$Fe^{2+} - O \rightarrow Fe^{3+} - O^- \quad (R5)$$

$$Fe^{3+} - O^- + N_2O \rightarrow Fe^{2+} - O_2 + N_2 \quad (R6)$$

$$Fe^{2+} - O_2 \rightarrow Fe^{2+} + O_2 \quad (R7)$$

For the ODHP with nitrous oxide, the circumstances are somewhat more complicated. The direct reaction between propane and gaseous oxygen results in the formation of CO_x as main products [13,51], so propane should react with adsorbed oxygen species to produce propylene with high selectivity. Indeed, when Fe-ZSM-5-G was subjected to an oxidation pretreatment in nitrous oxide at 773 K, it exhibited higher initial propene selectivity than that without such pretreatment, as shown in Fig. S10. The oxidation pretreatment can eliminate the induction period of Fe-ZSM-5-G in ODHP by the introduction of the thermally stable oxygen species

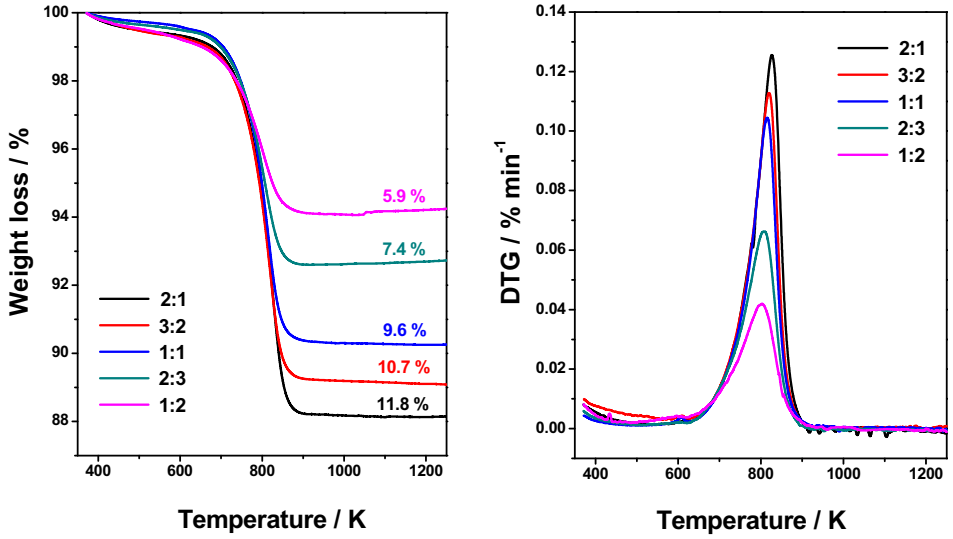

Fig. 11. TG-DTG analyses of Fe-ZSM-5-G catalysts after the ODHP with nitrous oxide at 748 K for 400 min with different N_2O/C_3H_8 ratios.

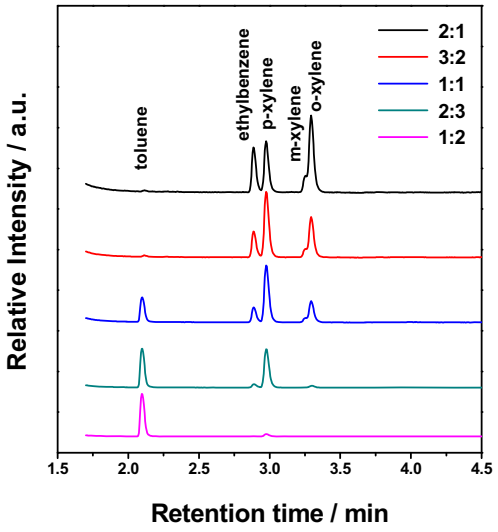

Fig. 12. GC–MS analysis of occluded organic species in Fe-ZSM-5-G catalysts after the ODHP with nitrous oxide at 748 K for 400 min with different N_2O/C_3H_8 ratios.

O^-, which confirms the involvement of these species in the reaction. Moreover, the formation of oxygen species, *i.e.* O^-, appears to be relatively slow in the reaction. Considering that the chemisorption of nitrous oxide on Fe-ZSM-5-G is a very fast step, the oxidation of ferrous sites to ferric sites by deposited oxygen species (R5) might be the rate determining step in the whole reaction process.

However, it is very difficult to judge how propane participates in the reaction. The results from in situ DRIFT spectroscopy (Figs. 6 and 7) reveal that similar organic species are formed upon propane activation on clean ferrous sites (Fe^{2+}) and ferrous sites pre-treated with nitrous oxide at 748 K (Fe^{3+}–O^-) or under in situ reaction conditions (C_3H_8–N_2O co-feeding). Therefore, we propose that gaseous propane directly reacts with adsorbed O^- via a simple Eley–Rideal mechanism (R8), similar to the reaction between adsorbed O^- and gaseous nitrous oxide.

$$Fe^{3+} - O^- + C_3H_8 \rightarrow Fe^{2+} + C_3H_6 + H_2O \quad \text{(R8)}$$

The propylene product can further react with adsorbed oxygen species to form CO_x (R9), most probably via allyl alcohol, acrolein and bicarbonate as reaction intermediates (TPSR results in Fig. 4 and DRIFT spectra in Figs. 6 and 7).

$$Fe^{3+} - O^- + C_3H_6 \rightarrow \cdots \rightarrow Fe^{2+} + CO_x + H_2O \quad \text{(R9)}$$

4.2. Deactivation mechanism for ODHP with nitrous oxide

Catalyst deactivation is a vital issue in ODHP with N_2O and it has been proposed to be related with the formation of coke during reaction. In the present study, the formation of organic species is indeed observed and the color of catalyst samples gradually changes from light yellow to dark gray with reaction progress. TG analysis results (Fig. 10) reveal that the accumulation rate of organic species ("coke") is very much dependent on the relative partial pressure of propane and nitrous oxide, *i.e.* the N_2O/C_3H_8 ratio. Lower N_2O/C_3H_8 ratios result in lower accumulation rates of organic species and subsequent lower deactivation rates (Fig. 8). Results from in situ DRIFT spectroscopy indicate that the adsorbates present during ODHP with N_2O are quite similar with different N_2O/C_3H_8 ratios (Fig. S11). In literature reports on ODHP with N_2O, reaction conditions of $N_2O/C_3H_8 = 1$ [4–8,12] or $N_2O/C_3H_8 > 1$ [9,10] were employed. Notably, we find that a very stable propylene yield can be obtained with N_2O/C_3H_8 ratio of <1 in the present study. Generally, excess oxidant, *i.e.* nitrous oxide, is helpful to suppress the deposition of coke species on the surface of catalyst and to increase the lifetime of catalyst. However, excess nitrous oxide will decompose to oxygen and nitrogen at elevated temperature, probably via another pathway since the formation of Fe^{2+} might be slow. The decomposition product oxygen will non-selectively oxidize propane to CO_x and then damage the propylene yield. The oxygen can also react with the desired product propylene, which not only damages the propylene yield but also accelerates the apparent deactivation of catalyst. Taking all these factors into consideration, a low N_2O/C_3H_8 ratio of <1 is believed to be more suitable for our Fe-ZSM-5-G catalyst and under our reaction conditions. Typically, extraordinary stability in ODHP with nitrous oxide (~40 h) is obtained over Fe-ZSM-5-G with a N_2O/C_3H_8 ratio of 1:2 (Fig. 10).

During the reaction of ODHP with nitrous oxide over Fe-ZSM-5-G, traces of aromatics (MB, DMB and EB) can be detected in the product outlet (Fig. 4). Results from GC–MS analysis of

occluded organic species in the spent catalyst confirm the deposition of aromatics as main coke species during ODHP with nitrous oxide. It is very interesting to note that the kinetic diameter of organic species significantly increases with the N_2O/C_3H_8 ratio (Fig. 12). Undoubtedly, the deposition of organic species with larger kinetic diameter on the catalyst will lead to more significant blocking of the channels, and therefore, accelerate the coking rate, as confirmed by the TG analysis results (Fig. 11). Herein, the formation of organic species with diameter larger than that of MFI channels, *e.g.* o-xylene and m-xylene, should be a key point for the deactivation. After 400 min time-on-stream, significant catalyst deactivation is observed with N_2O/C_3H_8 ratios of 1:1, 3:2 and 2:1, wherein o-xylene and m-xylene could be detected as occluded organic species in the channels of Fe-ZSM-5-G. In contrast, no significant catalyst deactivation is ob served with N_2O/C_3H_8 ratios of 2:3 and 1:2 after 400 min time-on-stream, wherein toluene and p-xylene are detected as dominant occluded organic species. Only in the deactivated state obtained after 72 h time-on-stream at a N_2O/C_3H_8 ratio of 1:2 (cf. Fig. 10), organic species with diameter larger than the channels of MFI structure, *i.e.* o-xylene, m-xylene and durene, were detected in the Fe-ZSM-5-G catalyst (Fig. S12).

5. Conclusions

In the present study, Fe-ZSM-5 is prepared via solid-state exchange method using ferrocene as iron precursor and employed as a model catalyst to investigate the reaction and deactivation mechanism of the ODHP with nitrous oxide. The iron species are well characterized by a series of techniques, and highly isolated Fe–O–Al species, accounting for *ca.* 60% of the total iron species, were detected in Fe-ZSM-5 after calcination at 1073 K. The reaction mechanism of the ODHP with nitrous oxide over this Fe-ZSM-5 model catalyst is investigated by means of temperature-programmed experiments and in situ DRIFT spectroscopy. The reaction between adsorbed oxygen species and gaseous propane is the key step leading to propylene production, and the simplified reaction pathway is proposed as follows.

$$Fe^{2+} + N_2O \rightarrow N_2 + Fe^{2+} - O$$

$$Fe^{2+} - O \rightarrow Fe^{3+} - O^-$$

$$Fe^{3+} - O^- + C_3H_8 \rightarrow Fe^{2+} + C_3H_6 + H_2O$$

The oxygen species O^- resulting from the reoxidation of Fe^{2+}–O–Al sites with N_2O is surprisingly stable and highly selective.

The deposition of organic species in Fe-ZSM-5 catalyst during the ODHP with nitrous oxide is confirmed by TG analysis and the dominant organic species are determined to be alkylbenzenes by GC–MS analysis. For the first time, it is found that the accumulation rate and the specific constitution of alkylbenzene species are very much dependent on the N_2O/C_3H_8 ratio, which subsequently influences the deactivation behavior of Fe-ZSM-5 catalyst in the ODHP with nitrous oxide. Under our reaction conditions, lower N_2O/C_3H_8 ratio is advantageous to get longer catalyst lifetime. The formation of alkylbenzenes with diameter larger than the channels of MFI structure, *e.g.* o-xylene and m-xylene, is observed as the direct reason for the catalytic deactivation.

Acknowledgements

This work is financially supported by the National Natural Science Foundation of China (21373119) and the Ministry of Education of China (NCET-11-0251, IRT13R30, IRT13022). The support from 111 Project (B12015) and the Collaborative Innovation Center of Chemical Science and Engineering (Tianjin) is also acknowledged.

Appendix A. Supplementary data

Supplementary data associated with this article can be found, in the online version, at http://dx.doi.org/10.1016/j.micromeso.2014.07.032.

References

[1] F. Cavani, N. Ballarini, A. Cericola, Catal. Today 127 (2007) 113–131.
[2] K. Nowińska, A. Wacław, A. Izbińska, Appl. Catal. A 243 (2003) 225–236.
[3] R. Bulánek, B. Wichterlová, K. Novoveská, V. Kreibich, Appl. Catal. A 264 (2004) 13–22.
[4] J. Pérez-Ramírez, A. Gallardo-Llamas, J. Catal. 223 (2004) 382–388.
[5] E.V. Kondratenko, J. Pérez-Ramírez, Appl. Catal. A 267 (2004) 181–189.
[6] J. Pérez-Ramírez, A. Gallardo-Llamas, Appl. Catal. A 279 (2005) 117–123.
[7] J. Pérez-Ramírez, A. Gallardo-Llamas, J. Phys. Chem. B 109 (2005) 20529–20538.
[8] O. Sánchez-Galofré, Y. Segura, J. Pérez-Ramírez, J. Catal. 249 (2007) 123–133.
[9] W. Wei, J.A. Moulijn, G. Mul, J. Catal. 262 (2009) 1–8.
[10] J. Kowalska-Kus, A. Held, K. Nowinska, Catal. Lett. 136 (2010) 199–208.
[11] A. Ates, C. Hardacre, A. Goguet, Appl. Catal. A 441 (2012) 30–41.
[12] P. Sazama, N.K. Sathu, E. Tabor, B. Wichterlová, Š. Sklenák, Z. Sobalík, J. Catal. 299 (2013) 188–203.
[13] G. Wu, F. Hei, N. Guan, L. Li, Catal. Sci. Technol. 5 (2013) 1333–1342.
[14] B.R. Wood, J.A. Reimer, A.T. Bell, J. Catal. 209 (2002) 151–158.
[15] J. Pérez-Ramírez, J. Catal. 227 (2004) 512–522.
[16] A. Heyden, B. Peters, A.T. Bell, F.J. Keil, J. Phys. Chem. B 109 (2005) 1857–1873.
[17] G.D. Pirngruber, P.K. Roy, Catal. Today 110 (2005) 199–210.
[18] K. Sun, H. Xia, E. Hensen, R. van Santen, C. Li, J. Catal. 238 (2006) 186–195.
[19] E. Berrier, O. Ovsitser, E.V. Kondratenko, M. Schwidder, W. Grünert, A. Brückner, J. Catal. 249 (2007) 67–78.
[20] G. Wu, F. Hei, N. Zhang, N. Guan, L. Li, W. Grünert, Appl. Catal. A 468 (2013) 230–239.
[21] J. Long, X. Wang, Z. Ding, Z. Zhang, H. Lin, W. Dai, X. Fu, J. Catal. 264 (2009) 163–174.
[22] K. Hadjiivanov, Catal. Rev. Sci. Eng. 42 (2000) 71–144.
[23] A. Zecchina, M. Rivallan, G. Berlier, C. Lamberti, G. Ricchiardi, Phys. Chem. Chem. Phys. 9 (2007) 3483–3499.
[24] G. Berlier, C. Lamberti, M. Rivallanw, G. Mul, Phys. Chem. Chem. Phys. 12 (2010) 358–364.
[25] L.J. Lobree, I.-C. Hwang, J.A. Reimer, A.T. Bell, J. Catal. 186 (1999) 242–253.
[26] G.D. Pirngruber, P.K. Roy, R. Prins, J. Catal. 246 (2007) 147–157.
[27] G. Mul, J. Pérez-Ramírez, F. Kapteijn, J.A. Moulijn, Catal. Lett. 80 (2002) 129–138.
[28] E.J.M. Hensen, Q. Zhu, R.A. van Santen, J. Catal. 220 (2003) 260–264.
[29] R.W. Joyner, M. Stockenhuber, J. Phys. Chem. B 103 (1999) 5963–5976.
[30] M. Lezcano, V.I. Kovalchuk, J.L. d'Itri, Kinet. Catal. 42 (2001) 104–111.
[31] L. Kiwi-Minsker, D.A. Bulushev, A. Renken, J. Catal. 219 (2003) 273–285.
[32] K. Sun, H. Xia, Z. Feng, R. van Santen, E. Hensen, C. Li, J. Catal. 254 (2008) 383–396.
[33] E.V. Kondratenko, J. Pérez-Ramírez, J. Phys. Chem. B 110 (2006) 22586–22595.
[34] Q. Zhang, Q. Guo, X. Wang, T. Shishido, Y. Wang, J. Catal. 239 (2006) 105–116.
[35] C. Zhang, R.A. Catlow, J. Catal. 259 (2008) 17–25.
[36] M. Yoshida, T. Nobukawa, S. Ito, K. Tomishige, K. Kunimori, J. Catal. 223 (2004) 454–464.
[37] G.I. Panov, A.K. Uriarte, M.A. Rodkin, V.I. Sobolev, Catal. Today 41 (1998) 365–385.
[38] T. Nobukawa, M. Yoshida, S. Kameoka, S. Ito, K. Tomishige, K. Kunimori, Catal. Today 93–95 (2004) 791–796.
[39] M. Che, A.J. Tench, Adv. Catal. 32 (1983) 1–148.
[40] K. Nakamoto, Infrared and Raman Spectra of Inorganic and Coordination Compounds, John Wiley, New York, 1997.
[41] L. Li, N. Guan, Microporous Mesoporous Mater. 117 (2009) 450–457.
[42] G. Wu, S. Jiang, L. Li, F. Zhang, Y. Yang, N. Guan, M. Mihaylov, H. Knözinger, Microporous Mesoporous Mater. 135 (2010) 2–8.
[43] K. Hadjiivanov, G. Busca, Langmuir 10 (1994) 4534–4541.
[44] M. Bjørgen, S. Akyalcin, U. Olsbye, S. Benard, S. Kolboe, S. Svelle, J. Catal. 275 (2010) 170–180.
[45] W. Dai, X. Wang, G. Wu, N. Guan, M. Hunger, L. Li, ACS Catal. 1 (2011) 292–299.
[46] NIST Chemistry Web book, http://webbook.nist.gov/chemistry.
[47] T. Mole, J.R. Anderson, G. Creer, Appl. Catal. 17 (1985) 141–156.
[48] J. O'Brien-Abraham, M. Kanezashi, Y.S. Lin, J. Membr. Sci. 320 (2008) 505–513.
[49] H. Sakai, T. Tomita, T. Takahashi, Sep. Purif. Technol. 25 (2001) 297–306.
[50] A. Heyden, N. Hansen, A.T. Bell, F.J. Keil, J. Catal. 233 (2005) 26–35.
[51] K. Novoveská, R. Bulánek, B. Wichterlová, Catal. Today 100 (2005) 315–319.